Relativistic quasiparticle random-phase approximation calculation of total muon capture rates

T. Marketin, N. Paar, T. Nikšić, and D. Vretenar

Physics Department, Faculty of Science, University of Zagreb, 10000 Zagreb, Croatia

The relativistic proton-neutron quasiparticle random phase approximation (pn-RQRPA) is applied in the calculation of total muon capture rates on a large set of nuclei from ^{12}C to ^{244}Pu, for which experimental values are available. The microscopic theoretical framework is based on the relativistic Hartree-Bogoliubov (RHB) model for the nuclear ground state, and transitions to excited states are calculated using the pn-RQRPA. The calculation is fully consistent, i.e., the same interactions are used both in the RHB equations that determine the quasiparticle basis, and in the matrix equations of the pn-RQRPA. The calculated capture rates are sensitive to the in-medium quenching of the axial-vector coupling constant. By reducing this constant from its free-nucleon value $g_A = 1.262$ by 10% for all multipole transitions, the calculation reproduces the experimental muon capture rates to better than 10% accuracy.

I. INTRODUCTION

Semileptonic weak interaction processes in nuclei are very sensitive to detailed properties of nuclear ground states and excitations. In astrophysical applications, in particular, weak interaction rates (β-decay half-lives, neutrino-nucleus cross sections, electron capture rates) must be calculated for hundreds of isotopes. Many of those are located far from the valley of β-stability, and thus not easily accessible in experiments. For a consistent description, reliable predictions and extrapolations of these processes it is, therefore, essential to employ a consistent theoretical framework based on microscopic nuclear structure models.

At present the framework of nuclear energy density functionals (NEDF) provides the most complete description of ground-state properties and collective excitations over the whole nuclide chart. At the level of practical applications the NEDF framework is realized in terms of self-consistent mean-field (SCMF) models. With a small set of universal parameters adjusted to data, the SCMF approach has achieved a high level of accuracy in the description of structure properties over the whole chart of nuclides, from relatively light systems to superheavy nuclei, and from the valley of β-stability to the particle drip-lines [1,2].

In a series of recent studies we have used a fully consistent microscopic approach based on relativistic energy density functionals to analyze β-decay half-lives of neutron-rich nuclei [3,4], and to model inclusive charged-current neutrino-nucleus reactions [5]. In this framework nuclear ground states are described using the relativistic Hartree-Bogoliubov (RHB) model [2], and transitions to excited nuclear states are calculated in the relativistic quasiparticle random-phase approximation (RQRPA) [6,7]. There are important advantages in using functionals with manifest covariance, the most obvious being the natural inclusion of the nucleon spin degree of freedom. The resulting nuclear spin-orbit potential has the correct empirical strength and isospin dependence. This is, of course, especially important in the description of excitations in the spin-isospin channel, e.g., semileptonic weak interaction processes. In addition, by employing a single

universal effective interaction in modeling both ground-state properties and multipole excitations in various mass regions of the chart of nuclides, the calculation of weak-interaction rates is essentially parameter free, and can be extended to regions of nuclei far from stability, including those on the r-process path.

To successfully extend a particular microscopic approach to regions of unknown nuclei far from stability, it is necessary to perform extensive tests and compare results with available data. Reliable prediction of weak interaction rates, in particular, require a fully consistent description of the structure of ground states and multipole excitations. For instance, calculated β-decay half-lives are very sensitive to low-energy Gamow-Teller transitions, but can only test excitations of lowest multipoles. Higher multipoles are excited in neutrino-nucleus reactions in the low-energy range below 100 MeV, and these reactions could play an important role in many astrophysical processes, including stellar nucleosynthesis. There is, however, only few data on neutrino-nucleus reactions, and these are limited to relatively light nuclei. Much more data is available for total muon capture rates. Muon capture on stable nuclei has been studied in details since many years, both experimentally and theoretically [8–11]. In this process the momentum transfer is of the order of the muon mass and, therefore, the calculation of total muon capture rates presents an excellent test of models that are also used in studies of low-energy neutrino-nucleus reactions.

In this work we test the fully consistent RHB plus proton-neutron RQRPA model in the calculation of total muon capture rates on a large set of nuclei from ^{12}C to ^{244}Pu, for which experimental values are available [12]. Previous calculation of muon capture rates on selected nuclei using the RPA approach include the consistent Hartree-Fock (HF) RPA model [13,14], in which the HF mean field and the particle-hole interaction result from the same Skyrme effective force, and a series of studies [15–18] in which both the continuum and standard RPA were used, and the effect of quenching of axial-vector coupling was analyzed. The present analysis parallels the recent study by Zinner, Langanke, and Vogel [18], where the nonrelativistic RPA was used to systematically

calculate muon capture rates for nuclei with $6 \leqslant Z \leqslant 94$. There are, however, significant differences between the two approaches. The model employed in Refs. [15–18] uses a phenomenological Woods-Saxon potential to generate the basis of single-nucleon states. The strength of the potential is adjusted to experimental proton and neutron separation energies in individual nuclei. In a second step the RPA with a phenomenological Landau-Migdal residual interaction is used to calculate nuclear excitations. The present approach, as already emphasized above, is fully consistent: both the basis of single-nucleon states and multipole excitations of nuclei are calculated from the same energy density functional or nuclear effective interaction. Results will be compared with data and discussed in relation to those reported in Ref. [18]. In particular, we will consider the important issue of quenching of the axial-vector strength.

II. THEORETICAL FRAMEWORK

The capture of a negative muon from the atomic $1s$ orbit on a nucleus (Z, N),

$$\mu^- + (Z, N) \longrightarrow \nu_\mu + (Z - 1, N + 1)^*, \quad (1)$$

presents a simple semileptonic reaction that proceeds via the charged current of the weak interaction. Detailed expressions for the reaction rates and the transition matrix elements can be found in Refs. [11,19,20]. The capture rate reads

$$\omega_{fi} = \frac{\Omega \nu^2}{2\pi} \sum_{\text{lepton spins}} \frac{1}{2J_i + 1} \sum_{M_i} \sum_{M_f} |\langle f| \hat{H}_W |i \rangle|^2, \quad (2)$$

where Ω denotes the quantization volume and ν is the muon neutrino energy. The Hamiltonian $\hat{H}_W$ of the weak interaction is expressed in the standard current-current form, i.e., in terms of the nucleon $\mathcal{J}_\lambda(\boldsymbol{x})$ and lepton $j_\lambda(\boldsymbol{x})$ currents

$$\hat{H}_W = -\frac{G}{\sqrt{2}} \int d\boldsymbol{x} \, \mathcal{J}_\lambda(\boldsymbol{x}) j^\lambda(\boldsymbol{x}), \quad (3)$$

and the transition matrix elements read

$$\langle f| \hat{H}_W |i \rangle = -\frac{G}{\sqrt{2}} l_\lambda \int d^3x \frac{\phi_{1s}(\boldsymbol{x})}{1/\sqrt{\Omega}} e^{-i\boldsymbol{q}\cdot\boldsymbol{x}} \langle f| \mathcal{J}^\lambda(\boldsymbol{x}) |i \rangle. \quad (4)$$

$\phi_{1s}(\boldsymbol{x})$ is the muon $1s$ wave function, the four-momentum transfer is $q \equiv (q_0, \boldsymbol{q})$, and the multipole expansion of the leptonic matrix element $l_\lambda e^{-i\boldsymbol{q}\cdot\boldsymbol{x}}$ determines the operator structure for the nuclear transition matrix elements [11,19,20]. The expression for the muon capture rate is given by

$$\omega_{fi} = \frac{2G^2 \nu^2}{(1 + \nu/M_T)} \frac{1}{2J_i + 1} \left\{ \sum_{J=0}^{\infty} |\langle J_f \| \phi_{1s} (\hat{\mathcal{M}}_J - \hat{\mathcal{L}}_J) \| J_i \rangle|^2 \right.$$
$$\left. + \sum_{J=1}^{\infty} |\langle J_f \| \phi_{1s} (\hat{\mathcal{T}}_J^{el} - \hat{\mathcal{T}}_J^{\text{mag}}) \| J_i \rangle|^2 \right\}, \quad (5)$$

where G is the weak coupling constant, the phase-space factor $(1 + \nu/M_T)^{-1}$ accounts for the nuclear recoil, and M_T is

the mass of the target nucleus. The nuclear transition matrix elements between the initial state $|J_i\rangle$ and final state $|J_f\rangle$, correspond to the charge $\hat{\mathcal{M}}_J$, longitudinal $\hat{\mathcal{L}}_J$, transverse electric $\hat{\mathcal{T}}_J^{EL}$, and transverse magnetic $\hat{\mathcal{T}}_J^{\text{MAG}}$ multipole operators:

(i) the Coulomb operator

$$\hat{\mathcal{M}}_{JM}(\boldsymbol{x}) = F_1^V M_J^M(\boldsymbol{x}) - i \frac{\kappa}{m_N}$$
$$\times \left[F_A \Omega_J^M(\boldsymbol{x}) + \frac{1}{2}(F_A - m_\mu F_P) \Sigma_J''^M(\boldsymbol{x}) \right], \quad (6)$$

(ii) the longitudinal operator

$$\hat{\mathcal{L}}_{JM}(\boldsymbol{x}) = \frac{q_0}{\kappa} F_1^V M_J^M(\boldsymbol{x}) + i F_A \Sigma_J''^M(\boldsymbol{x}), \quad (7)$$

(iii) the transverse electric operator

$$\hat{\mathcal{T}}_{JM}^{el}(\boldsymbol{x}) = \frac{\kappa}{m_N} \left[F_1^V \Delta_J'^M(\boldsymbol{x}) + \frac{1}{2} \mu^V \Sigma_J^M(\boldsymbol{x}) \right]$$
$$+ i F_A \Sigma_J'^M(\boldsymbol{x}), \quad (8)$$

(iv) and the transverse magnetic operator

$$\hat{\mathcal{T}}_{JM}^{\text{mag}}(\boldsymbol{x}) = -i \frac{\kappa}{m_N} \left[F_1^V \Delta_J^M(\boldsymbol{x}) - \frac{1}{2} \mu^V \Sigma_J'^M(\boldsymbol{x}) \right]$$
$$+ F_A \Sigma_J^M(\boldsymbol{x}), \quad (9)$$

where all the form factors are functions of q^2, and $\kappa = |\boldsymbol{q}|$. These multipole operators contain seven basic operators expressed in terms of spherical Bessel functions, spherical harmonics, and vector spherical harmonics [19]. By assuming conserved vector current (CVC), the standard set of form factors reads [21]

$$F_1^V(q^2) = \left[1 + \left(\frac{q}{840\,\text{MeV}} \right)^2 \right]^{-2}, \quad (10)$$

$$\mu^V(q^2) = 4.706 \left[1 + \left(\frac{q}{840\,\text{MeV}} \right)^2 \right]^{-2}, \quad (11)$$

$$F_A(q^2) = -1.262 \left[1 + \left(\frac{q}{1032\,\text{MeV}} \right)^2 \right]^{-2}, \quad (12)$$

$$F_P(q^2) = \frac{2m_N F_A(q^2)}{q^2 + m_\pi^2}. \quad (13)$$

The muon capture rates are evaluated using Eq. (5), with the transition matrix elements between the initial and final states determined in a fully microscopic theoretical framework based on the relativistic Hartree-Bogoliubov (RHB) model for the nuclear ground state, and excited states are calculated using the relativistic quasiparticle random phase approximation (RQRPA). The RQRPA has been formulated in the canonical single-nucleon basis of the relativistic Hartree-Bogoliubov (RHB) model in Ref. [6], and extended to the description of charge-exchange excitations (proton-neutron RQRPA) in Ref. [7]. In addition to configurations built from two-quasiparticle states of positive energy, the relativistic QRPA configuration space must also include pair-configurations

formed from the fully or partially occupied states of positive energy and empty negative-energy states from the Dirac sea. The RHB+RQRPA model is fully consistent: in the particle-hole (ph) channel effective Lagrangians with density-dependent meson-nucleon couplings are employed, and pairing (pp) correlations are described by the pairing part of the finite range Gogny interaction. Both in the ph and pp channels, the same interactions are used in the RHB equations that determine the canonical quasiparticle basis, and in the matrix equations of the RQRPA. In this work we use one of the most accurate meson-exchange density-dependent relativistic mean-field effective interactions—DD-ME2 [22] in the ph channel, and the finite range Gogny interaction D1S [23] in the pp channel.

The spin-isospin-dependent interaction terms are generated by the π- and ρ-meson exchange. Although the direct one-pion contribution to the nuclear ground state vanishes at the mean-field level because of parity conservation, the pion must be included in the calculation of spin-isospin excitations. The particle-hole residual interaction of the *pn*-RQRPA is derived from the Lagrangian density:

$$\mathcal{L}_{\pi+\rho}^{\text{int}} = -g_\rho \bar{\psi} \gamma^\mu \vec{\rho}_\mu \vec{\tau} \psi - \frac{f_\pi}{m_\pi} \bar{\psi} \gamma_5 \gamma^\mu \partial_\mu \vec{\pi} \vec{\tau} \psi, \quad (14)$$

where vectors in isospin space are denoted by arrows. For the density-dependent coupling strength of the ρ-meson to the nucleon we choose the value that is used in the DD-ME2 effective interaction [22], and the standard value for the pseudovector pion-nucleon coupling is $f_\pi^2/4\pi = 0.08$, and $m_\pi = 138$ MeV. The derivative type of the pion-nucleon coupling necessitates the inclusion of the zero-range Landau-Migdal term, which accounts for the contact part of the nucleon-nucleon interaction

$$V_{\delta\pi} = g' \left(\frac{f_\pi}{m_\pi} \right)^2 \vec{\tau}_1 \vec{\tau}_2 \boldsymbol{\Sigma}_1 \cdot \boldsymbol{\Sigma}_2 \delta(\boldsymbol{r}_1 - \boldsymbol{r}_2), \quad (15)$$

with the parameter g' adjusted in such a way that the *pn*-RQRPA reproduces experimental values of Gamow-Teller resonance (GTR) excitation energies [7]. The precise value depends on the choice of the nuclear symmetry energy at saturation, and for the DD-ME2 effective interaction $g' = 0.52$ has been adjusted to the position of the GTR in ^{208}Pb. This value is kept constant for all nuclides calculated in this work.

In the evaluation of muon capture rates [Eq. (5)], for each transition operator $\hat{O}_J$ the matrix elements between the ground state of the even-even (N, Z) target nucleus and the final state are expressed in terms of single-particle matrix elements between quasiparticle canonical states, the corresponding occupation probabilities, and RQRPA amplitudes:

$$\langle J_f || \hat{O}_J || J_i \rangle = \sum_{pn} \langle p || \hat{O}^J || n \rangle \left(X_{pn}^J u_p v_n - Y_{pn}^J v_p u_n \right). \quad (16)$$

Transitions between the $|0^+\rangle$ ground state of a spherical even-even target nucleus and excited states in the corresponding odd-odd nucleus are considered. The total muon capture rate

is calculated from the expression:

$$\omega = 2G^2 \left\{ \sum_{J_f=0}^{\infty} \frac{v_f^2}{(1 + v_f/M_T)} |\langle J_f || \phi_{1s} (\hat{\mathcal{M}}_{J_f} - \hat{\mathcal{L}}_{J_f}) || 0^+ \rangle|^2 \right.$$
$$\left. + \sum_{J_f=1}^{\infty} \frac{v_f^2}{(1 + v_f/M_T)} |\langle J_f || \phi_{1s} (\hat{\mathcal{T}}_{J_f}^{el} - \hat{\mathcal{T}}_{J_f}^{\text{mag}}) || 0^+ \rangle|^2 \right\},$$
$$(17)$$

with the neutrino energy determined by the energy conservation relation

$$m_\mu - \epsilon_b + E_i = E_f + v_f, \quad (18)$$

where ϵ_b is the binding energy of the muonic atom.

For each nucleus the muon wave function and binding energy are calculated as solutions of the Dirac equation with the Coulomb potential determined by the self-consistent ground-state charge density. However, while the RHB single-nucleon equations are solved by expanding nucleon spinors and meson fields in terms of eigenfunctions of a spherically symmetric harmonic oscillator potential, the same method could not be used for the muon wave functions. The reason, of course, is that the muon wave functions extend far beyond the surface of the nucleus and, even using a large number of oscillator shells, solutions expressed in terms of harmonic oscillator basis functions do not converge. The Dirac equation for the muon is therefore solved in coordinate space using the method of finite elements with B-spline shape functions [24,25]. As an illustration, in Fig. 1 we plot the square of the 1*s* muon wave functions for ^{16}O, ^{40}Ca, ^{120}Sn, and ^{208}Pb. The solutions that correspond to self-consistent ground-state charge densities are compared with eigenfunctions of the Coulomb potential for the corresponding point-charge *Z*. For light nuclei the radial dependence of the 1*s* muon wave function is not very different from that of the point-charge Coulomb potential. With the increase of Z the muon is pulled into the nuclear Coulomb potential, and thus the magnitude of the 1*s* density inside the nucleus is reduced with respect to the point-charge value. To test our calculation of muon orbitals in the nuclear Coulomb potential, in Tables I and II the muon transition energies in Sn isotopes and in ^{208}Pb, respectively, are compared with available data [26,27]. The calculated transition energies are in good agreement with experimental values.

TABLE I. Calculated muon transition energies in tin isotopes (in units of keV), compared with available data [26].

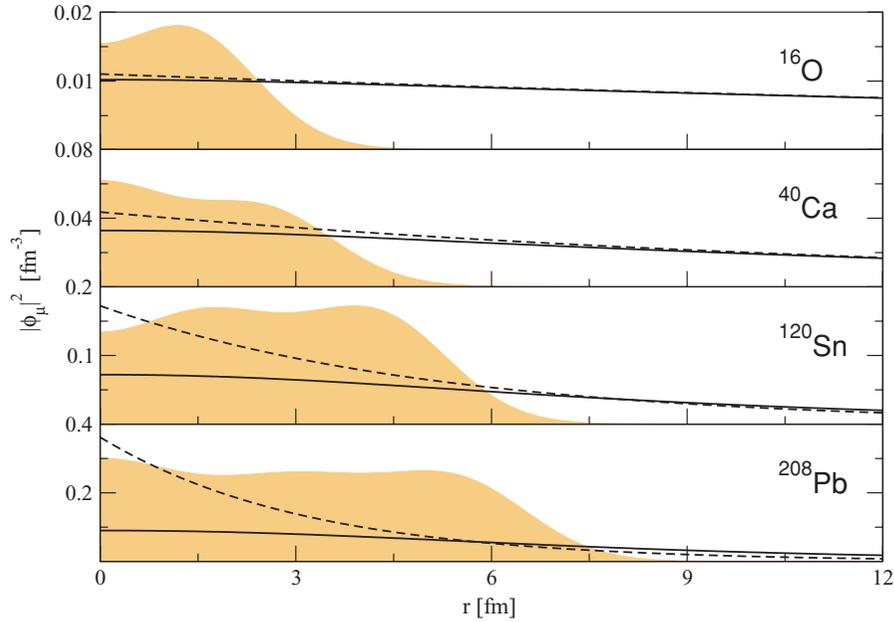|	$1p_{1/2} - 1s_{1/2}$		$1p_{3/2} - 1s_{1/2}$	
	Exp.	Calc.	Exp.	Calc.
^{112}Sn	3432	3439	3478	3485
^{114}Sn	3426	3432	3471	3478
^{116}Sn	3420	3427	3465	3472
^{118}Sn		3421		3466
^{120}Sn	3408	3415	3454	3460
^{122}Sn		3409		3454
^{124}Sn	3400	3404	3445	3450

FIG. 1. (Color online) The square of the $1s$ muon wave function in the Coulomb potentials of self-consistent ground-state charge densities of ^{16}O, ^{40}Ca, ^{120}Sn and ^{208}Pb (solid curves), compared to eigenfunctions of the Coulomb potential for the corresponding point charge Z (dashed curves). The figures also include the calculated charge densities of the four nuclei, scaled by arbitrary factors.

The effect of the finite distribution of ground-state charge densities on the calculated muon capture rates is illustrated in Fig. 2. For a large set of nuclei from ^{12}C to ^{244}Pu, we plot the ratio between calculated and experimental muon capture rates. This ratio is $\leqslant 1.5$ for all nuclei when the muon $1s$ wave functions are determined by self-consistent ground-state charge densities, whereas for point-charge Coulomb potentials one notes a distinct increase with Z, and $\omega_{\text{calc.}}/\omega_{\text{exp.}} \geqslant 4$ for the heaviest systems.

III. RESULTS FOR MUON CAPTURE RATES

The muon capture rates shown in Fig. 2 are calculated with the standard set of free nucleon weak form factors Eqs. (10)–(13) [21], i.e., the calculation does not include any in-medium quenching of the corresponding strength functions. Even with muon wave functions determined self-consistently by finite-charge densities, the resulting capture rates are larger than the corresponding experimental values by a factor ≈ 1.2–1.4. This is in contrast to the results of Ref. [18], where the experimental values have been reproduced to

TABLE II. Calculated muon transition energies in ^{208}Pb (in units of keV), in comparison with experimental values [27].

^{208}Pb	Exp.	Calc.
$1p_{3/2} - 1s_{1/2}$	5963	5956
$1p_{1/2} - 1s_{1/2}$	5778	5773
$1d_{3/2} - 1p_{1/2}$	2642	2633
$1d_{5/2} - 1p_{3/2}$	2501	2493
$1d_{3/2} - 1p_{3/2}$	2458	2450

better than 15% accuracy, using the free-nucleon weak form factors and residual interactions with a mild A dependency. In fact, it was shown that the calculated rates for the same residual interactions would be significantly below the data if the in-medium quenching of the axial-vector coupling constant is employed to other than the true Gamow-Teller (GT) amplitudes. Consequently, the calculations reported in Ref. [18] were performed with quenching only the GT part of the transition strength by a common factor $(0.8)^2 = 0.64$. It was concluded, however, that there is actually no need to apply any quenching to operators that contribute to the muon capture process, especially those involving single-nucleon transitions between major oscillator shells.

As already emphasized in the Introduction, although both calculations are based on the RPA framework, there are important differences between the model of Ref. [18], and the RHB+RQRPA approach employed in the present study. The main difference is probably the fact that the present calculation is fully consistent: for all nuclei both the basis of single-nucleon states and the multipole response are calculated using the same effective interaction, whereas in Ref. [18] the phenomenological Woods-Saxon potential was adjusted to individual nuclei and the strength of the residual Landau-Migdal force had a mild A-dependence.

In Fig. 3 we compare the ratios of the theoretical and experimental total muon capture rates for two sets of weak form factors. First, the rates calculated with the free nucleon weak form factors Eqs. (10)–(13) [21] (circles), and already shown in Fig. 2. The lower rates, denoted by diamonds, are calculated by applying the same quenching $g_A = 1.262 \rightarrow g_A = 1.135$ to all axial operators, i.e., g_A is reduced by 10% in all multipole channels. In the latter case the level of agreement is very good, with the mean deviation between theoretical and experimental values of only 6%. The factor 0.9 with which the free-nucleon g_A is multiplied is chosen in such a
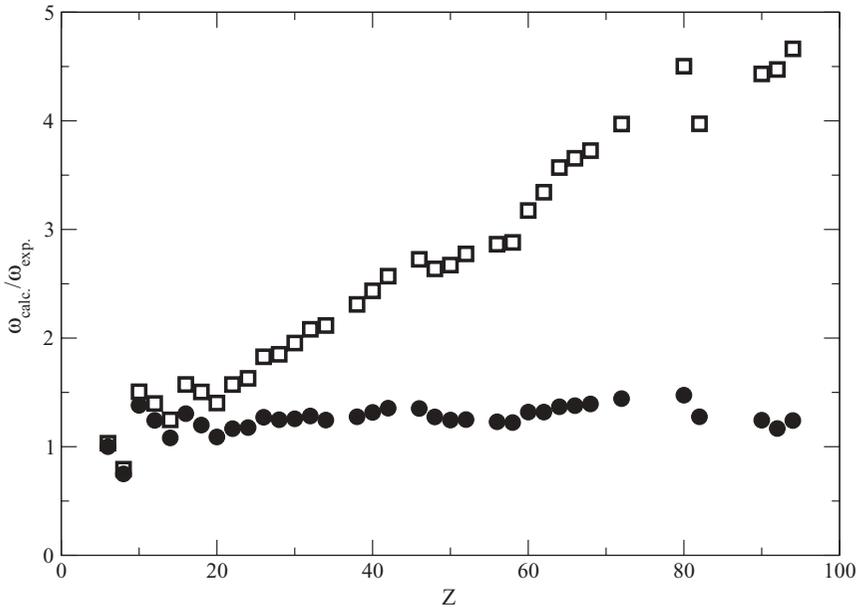
FIG. 2. Ratio of the calculated and experimental total muon capture rates, as function of the proton number Z. The theoretical values are calculated with muon $1s$ wave functions determined by self-consistent ground-state charge densities (filled circle symbols), and by the corresponding point-charge Coulomb potentials (squares).

way to minimize the deviation from experimental values for spherical, closed-shell medium-heavy and heavy nuclei. On the average the results are slightly better than those obtained in Ref. [18] (cf. Fig. 2 of [18]). Note, however, that in the calculation of Zinner, Langanke, and Vogel [18] only the true Gamow-Teller $0\hbar\omega$ transition strength was quenched, rather than the total strength in the 1^+ channel. In the present study considerably better results are obtained when the quenched value of the axial-vector coupling constants is used for all multipole operators. The reason to consider quenching the strength in all multipole channels, rather than just for the GT is, of course, that the axial form factor appears in all four operators Eqs. (6)–(9) that induce transitions between the initial and final states, irrespective of their multipolarity. Even more importantly, only a relatively small contribution

to the total capture rates actually comes from the GT channel 1^+. This is illustrated in Fig. 4, where we display the relative contributions of different multipole transitions to the RHB plus RQRPA muon capture rates in ^{16}O, ^{40}Ca, ^{120}Sn, and ^{208}Pb. For the two lighter $N = Z$ nuclei the dominant multipole transitions are $\lambda^\pi = 1^-$ and $\lambda^\pi = 2^-$ (spin-dipole). For the two heavier nuclei there are also significant contributions of the $\lambda^\pi = 1^+$ and $\lambda^\pi = 2^+$, especially for ^{208}Pb and for other heavy nuclei. Note that in heavy nuclei the $\lambda^\pi = 1^+$ multipole represents $2\hbar\omega$ transitions, rather than the $0\hbar\omega$ Gamow-Teller transitions.

Returning to Fig. 3, we notice that with a 10% quenching of the free-nucleon axial-vector coupling constant g_A, for medium-heavy and heavy nuclei the calculated capture rates are still slightly larger than the corresponding experimental

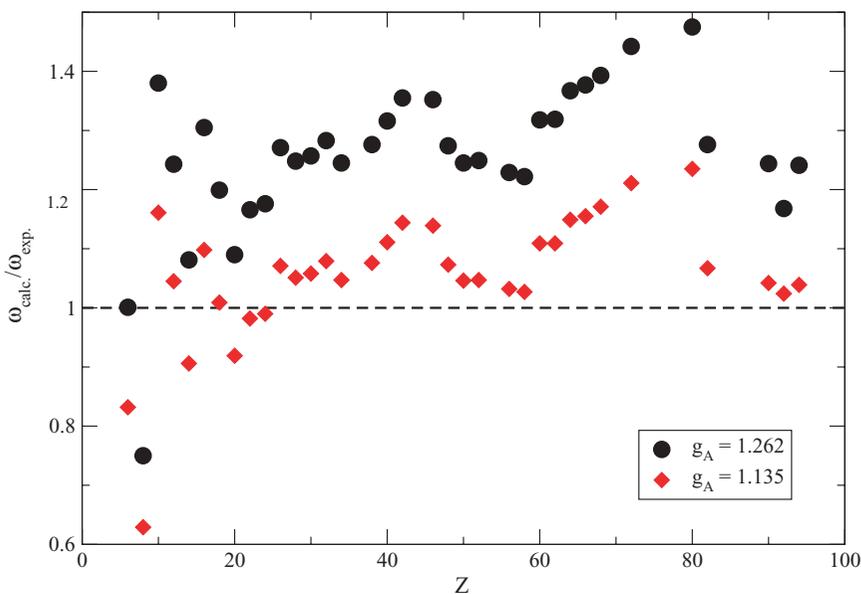
FIG. 3. (Color online) Ratio of the calculated and experimental total muon capture rates, as function of the proton number Z. Circles correspond to rates calculated with the free-nucleon weak form factors Eqs. (10)–(13) [21], and diamonds denote values obtained by quenching the free-nucleon axial-vector coupling constant $g_A = 1.262$ to $g_A = 1.135$ for all operators, i.e., in all multipole channels.

TABLE III. Experimental and calculated muon capture rates for natural elements and individual isotopes. The theoretical rates are calculated using the fully consistent RHB plus RQRPA framework with the DD-ME2 universal effective interaction, and with the quenching of the axial-vector coupling constant $g_A = 1.262 \rightarrow g_A = 1.135$ for all multipole operators. Values for naturally occuring elements (element symbol with no superscript) are weighted averages of capture rates on individual isotopes, using their natural abundances. Experimental values are from Ref. [12], unless otherwise stated. All rates are in units of 10^6 s^{-1}.

Nucleus	Exp.	Calc.	Nucleus	Exp.	Calc.	Nucleus	Exp.	Calc.	Nucleus	Exp.	Calc.
^{12}C	0.039	0.032	^{78}Se		6.644	^{122}Sn		9.645	^{164}Dy		13.540
^{16}O	0.103	0.065	^{80}Se		5.796	^{124}Sn		8.837	Dy	12.29	14.194
^{18}O	0.088	0.057	^{82}Se		4.935	Sn	10.44	10.923	^{166}Er		16.129
^{20}Ne	0.204	0.237	Se	5.681	5.950	^{126}Te		10.652	^{168}Er		14.949
^{24}Mg	0.484	0.506	^{86}Sr		8.885	^{128}Te		9.830	^{170}Er		13.912
^{28}Si	0.871	0.789	^{88}Sr		7.393	^{130}Te		9.068	Er	13.04	15.270
^{32}S	1.352	1.485	Sr	7.020	7.553	Te	9.270	9.706	^{178}Hf		16.434
^{40}Ar	1.355	1.368	^{90}Zr		9.874	^{132}Xe	9.4[b]	10.631	^{180}Hf		15.276
^{40}Ca	2.557	2.340	^{92}Zr		9.694	^{136}Xe	8.6[b]	8.625	Hf	13.03	15.783
^{44}Ca	1.793	1.851	^{94}Zr		8.792	^{136}Ba		11.461	^{182}W		17.259
^{48}Ca	1.214[a]	1.163	Zr	8.660	9.619	^{138}Ba		10.127	^{184}W		15.938
^{48}Ti	2.590	2.544	^{92}Mo		12.374	Ba	9.940	10.259	^{186}W		14.807
^{50}Cr	3.825	4.001	^{94}Mo		12.001	^{140}Ce		11.888	W	12.36	15.971
^{52}Cr	3.452	3.419	^{96}Mo		10.933	^{142}Ce		12.142	^{198}Hg		17.369
^{54}Cr	3.057	3.065	^{98}Mo		9.804	Ce	11.60	11.917	^{200}Hg		16.227
Cr	3.472	3.483	Mo	9.614	10.995	^{142}Nd		14.043	^{202}Hg		15.205
^{56}Fe	4.411	4.723	^{104}Pd		13.182	^{144}Nd		14.288	^{204}Hg		13.993
^{58}Ni	6.110	6.556	^{106}Pd		11.912	^{146}Nd		12.981	Hg	12.74	15.733
^{60}Ni	5.560	5.610	^{108}Pd		10.795	Nd	12.50	13.861	^{206}Pb		15.717
^{62}Ni	4.720	4.701	^{110}Pd		9.821	^{148}Sm		15.425	^{208}Pb		13.718
Ni	5.932	6.234	Pd	10.00	11.391	^{150}Sm		14.132	Pb	13.45	14.348
^{64}Zn		6.862	^{110}Cd		12.960	^{152}Sm		13.451	^{232}Th	12.56	13.092
^{66}Zn		5.809	^{112}Cd		11.800	^{154}Sm		12.563	^{234}U	13.79	14.231
^{68}Zn		4.935	^{114}Cd		10.746	Sm	12.22	13.554	^{236}U	13.09[c]	13.490
Zn	5.834	6.174	^{116}Cd		9.829	^{156}Gd		14.785	^{238}U	12.57[c]	12.872
^{70}Ge		6.923	Cd	10.61	11.381	^{158}Gd		13.573	^{242}Pu	12.90	13.554
^{72}Ge		5.970	^{116}Sn		12.395	^{160}Gd		12.460	^{244}Pu	12.40[d]	12.887
^{74}Ge		5.519	^{118}Sn		11.369	Gd	11.82	13.580			
Ge	5.569	6.011	^{120}Sn		10.486	^{162}Dy		14.917			

[a]From Ref. [28].
[b]From Ref. [29].
[c]From Ref. [30].
[d]From Ref. [31].

values, with the ratio $\omega_{\text{calc.}}/\omega_{\text{exp.}}$ typically around 1.1, whereas for several lighter nuclei considered here this ratio is actually less than 1 (cf. also Table III). Overall the best results, with $\omega_{\text{calc.}}/\omega_{\text{exp.}} \approx 1$, are obtained near closed shells. The characteristic arches between closed shells can probably be attributed to deformation effects, not taken into account in our RHB+RQRPA model. In addition to the DD-ME2 interaction, we have also carried out a full calculation of total capture rates from ^{12}C to ^{244}Pu, using the density- and momentum-dependent relativistic effective interaction D3C*. In the study of β-decay half-lives of Ref. [4], this interaction was constructed with the aim to enhance the effective (Landau) nucleon mass, and thus improve the RQRPA description of β-decay rates. When D3C* is used to calculate muon capture rates, some improvement is obtained only locally, for certain regions of Z, whereas in other regions ($Z \approx 50$ and $Z \geqslant 82$) the results are not as good as those obtained with DD-ME2.

The overall quality of the agreement between theoretical and experimental capture rates is slightly better with DD-ME2.

The calculated total muon capture rates for natural elements and individual isotopes are also collected in Table III, and compared with available data [12]. In particular, the calculation nicely reproduces the empirical isotopic dependence of the capture rates [8], i.e., for a given proton number Z the rates decrease with increasing neutron number, because of the gradual blocking of available neutron levels. The isotopic trend is also illustrated in Fig. 5, where we plot the experimental and theoretical total muon capture rates on Ca, Cr, and Ni nuclei. The latter correspond to the quenching $g_A = 1.262 \rightarrow g_A = 1.135$ for all multipole operators.

In conclusion, we have tested the RHB plus proton-neutron RQRPA model in the calculation of total muon capture rates on a large set of nuclei from ^{12}C to ^{244}Pu. The calculation is fully consistent, the same universal effective interactions
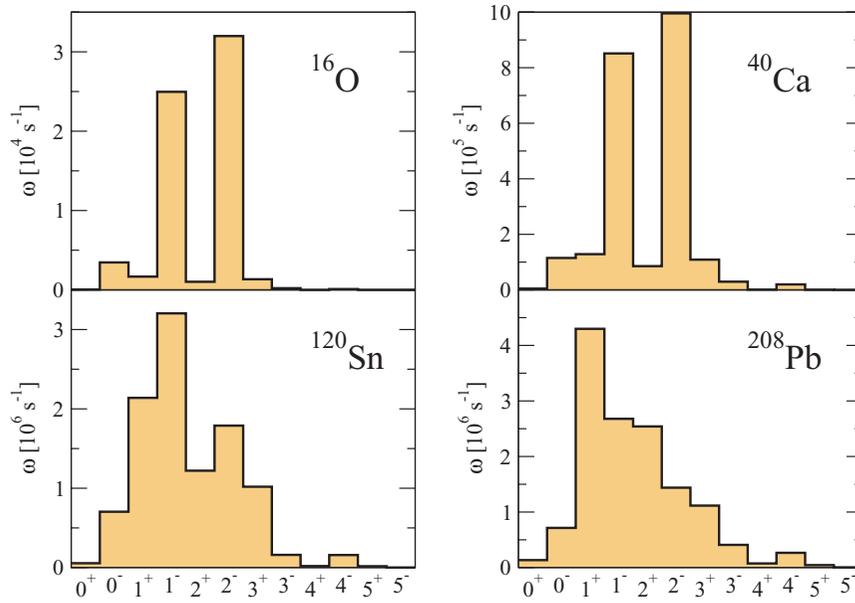
FIG. 4. (Color online) Relative contributions of different multipole transitions to the RHB plus RQRPA total muon capture rates in ^{16}O, ^{40}Ca, ^{120}Sn and ^{208}Pb.

are used both in the RHB equations that determine the quasiparticle basis, and in the matrix equations of the RQRPA. The calculated capture rates are sensitive to the in-medium quenching of the axial-vector coupling constant. By reducing this constant from its free-nucleon value $g_A = 1.262$ to the effective value $g_A = 1.135$ for all multipole transitions, i.e., with a quenching of approximately 10%, the experimental muon capture rates are reproduced with an accuracy better than 10%. This result can be compared to recent RPA-based calculations [16–18], that reproduce the experimental values to better than 15%, using phenomenological potentials adjusted to individual nuclei and A-dependent residual interactions, but without applying any quenching to the operators responsible for the μ^- capture process. The test has demonstrated that the RHB plus QRPA model provides a consistent and accurate description of semileptonic weak interaction processes at finite momentum transfer in medium-heavy and heavy nuclei over a large Z-range. The fully consistent microscopic approach, based on modern relativistic nuclear energy density functionals, can be extended to other types of weak interaction processes (electron capture, neutrino-nucleus charge-exchange, and neutral-current reactions), and to regions of short-lived nuclei far from stability.
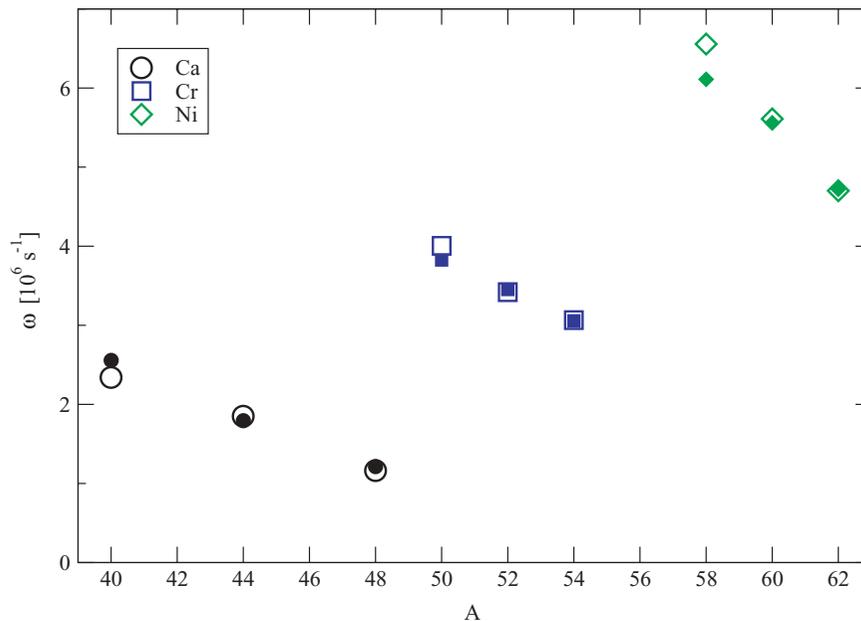
FIG. 5. (Color online) Total muon capture rates on Ca, Cr and Ni isotopes. Experimental rates (filled symbols) are compared to theoretical values (empty symbols), calculated using the fully consistent RHB plus RQRPA framework with the DD-ME2 universal effective interaction, and with the quenching of the axial-vector coupling constant $g_A = 1.262 \rightarrow g_A = 1.135$ for all multipole operators.

[1] M. Bender, P.-H. Heenen, and P.-G. Reinhard, Rev. Mod. Phys. **75**, 121 (2003).

[2] D. Vretenar, A. Afanasjev, G. Lalazissis, and P. Ring, Phys. Rep. **409**, 101 (2005).

[3] T. Nikšić, T. Marketin, D. Vretenar, N. Paar, and P. Ring, Phys. Rev. C **71**, 014308 (2005).

[4] T. Marketin, D. Vretenar, and P. Ring, Phys. Rev. C **75**, 024304 (2007).

[5] N. Paar, D. Vretenar, T. Marketin, and P. Ring, Phys. Rev. C **77**, 024608 (2008).

[6] N. Paar, P. Ring, T. Nikšić, and D. Vretenar, Phys. Rev. C **67**, 034312 (2003).

[7] N. Paar, T. Nikšić, D. Vretenar, and P. Ring, Phys. Rev. C **69**, 054303 (2004).

[8] H. Primakoff, Rev. Mod. Phys. **31**, 802 (1959).

[9] N. C. Mukhopadhyay, Phys. Rep. **30**, 1 (1977).

[10] D. Measday, Phys. Rep. **354**, 243 (2001).

[11] J. D. Walecka, in *Muon Physics*, edited by V. M. Hughes and C. S. Wu (Academic, New York, 1975).

[12] T. Suzuki, D. F. Measday, and J. P. Roalsvig, Phys. Rev. C **35**, 2212 (1987).

[13] N. Auerbach and A. Klein, Nucl. Phys. **A422**, 480 (1984).

[14] N. Auerbach, N. Van Giai, and O. K. Vorov, Phys. Rev. C **56**, R2368 (1997).

[15] E. Kolbe, K. Langanke, and P. Vogel, Phys. Rev. C **50**, 2576 (1994).

[16] E. Kolbe, K. Langanke, and P. Vogel, Phys. Rev. C **62**, 055502 (2000).

[17] N. T. Zinner, K. Langanke, K. Riisager, and E. Kolbe, Eur. Phys. J. A **17**, 625 (2003).

[18] N. T. Zinner, K. Langanke, and P. Vogel, Phys. Rev. C **74**, 024326 (2006).

[19] J. S. O'Connell, T. W. Donnely, and J. D. Walecka, Phys. Rev. C **6**, 719 (1972).

[20] J. D. Walecka, *Theoretical Nuclear and Subnuclear Physics* (Imperial College Press and World Scientific, London, 2004).

[21] T. Kuramoto, M. Fukugita, Y. Kohyama, and K. Kubodera, Nucl. Phys. **A512**, 711 (1990).

[22] G. A. Lalazissis, T. Nikšić, D. Vretenar, and P. Ring, Phys. Rev. C **71**, 024312 (2005).

[23] J. Berger, M. Girod, and D. Gogny, Comput. Phys. Commun. **63**, 365 (1991).

[24] J. A. McNeil, R. J. Furnstahl, E. Rost, and J. R. Shepard, Phys. Rev. C **40**, 399 (1989).

[25] C. deBoor, *A Practical Guide to Splines* (Springer, New York, 1978).

[26] C. Piller *et al.*, Phys. Rev. C **42**, 182 (1990).

[27] P. Bergem *et al.*, Phys. Rev. C **37**, 2821 (1988).

[28] H. O. U. Fynbo *et al.*, Nucl. Phys. **A724**, 493 (2003).

[29] T. N. Mamedov *et al.*, JETP Lett. **71**, 451 (2000).

[30] H. Hänscheid *et al.*, Z. Phys. A **335**, 1 (1990).

[31] P. David *et al.*, Z. Phys. A **330**, 397 (1988).